Observation of Giant Topological Hall Effect in Room-Temperature Ferromagnet $Cr_{0.82}Te$

Wei-Ting Miao(苗伟婷)[1,2], Wei-Li Zhen(甄伟立)[1*], Zhen Lu(陆振)[1], Heng-Ning Wang(王恒宁)[1], Jie Wang(王杰)[1], Qun Niu(牛群)[1*], and Ming-Liang Tian(田明亮)[1,2,3*]

[1]*Anhui Key Laboratory of Low-energy Quantum Materials and Devices, High Magnetic Field Laboratory, HFIPS, Chinese Academy of Sciences, Hefei 230031, China*
[2]*Science Island Branch, Graduate School of University of Science and Technology of China, Hefei 230026, China*
[3]*School of Physics and Optoelectronic Engineering, Anhui University, Hefei 230601, China*

(Received 13 March 2024; accepted manuscript online 15 May 2024)

Novel magnetic materials with non-trivial magnetic structures have led to exotic magnetic transport properties and significantly promoted the development of spintronics in recent years. Among them is the Cr_xTe_y family, the magnetism of which can persist above room temperature, thus providing an ideal system for potential spintronic applications. Here we report the synthesis of a new compound, $Cr_{0.82}Te$, which demonstrates a record-high topological Hall effect at room temperature in this family. $Cr_{0.82}Te$ displays soft ferromagnetism below the Curie temperature of 340 K. The magnetic measurement shows an obvious magneto-crystalline anisotropy with the easy axis located in the *ab* plane. The anomalous Hall effect can be well explained by a dominating skew scattering mechanism. Intriguing, after removing the normal Hall effect and anomalous Hall effect, a topological Hall effect can be observed up to 300 K and reaches up to 1.14 μΩ·cm at 10 K, which is superior to most topological magnetic structural materials. This giant topological Hall effect possibly originates from the noncoplanar spin configuration during the spin flop process. Our work extends a new Cr_xTe_y system with topological non-trivial magnetic structure and broad prospects for spintronics applications in the future.

DOI: 10.1088/0256-307X/41/6/067501

Magnetic materials are important for fundamental research and practical applications.[1] Magnetic random-access memory (MRAM) devices based on magnetic materials have greatly expanded the information storage capacity.[2] Furthermore, novel physical effects such as giant magnetoresistance (GMR), spin-transfer torque (STT), and spin-orbit torque (SOT) have been discovered due to the rapid development of spintronics.[3–5] However, the understanding of magnetic structures has largely remained focused on collinear or coplanar magnetic structures before the in-depth development of topological concepts in condensed matter physics. In recent years, topologically non-trivial magnetic structures, such as helical magnetic structures, skyrmions, and chiral magnetic bubbles have been discovered in magnetic materials with non-centrosymmetric or chiral magnetic properties.[6–10] These novel magnetic structures provide a rich platform for studying the competition of different magnetic interactions.[11] When itinerant electrons are coupled with these novel magnetic structures, a topological Hall effect (THE) may emerge, which has attracted intense attention in the spintronic community.[12–14] Taking advantage of the THE for transport detection of novel magnetic structures is of great importance, as the method is both simple and efficient.[15,16] Moreover, magnetic memory devices utilizing these structures are considered to have high information density and low power consumption.[17–19] However, the main challenge now is the rapid suppression of THE magnitude with increasing temperature.[20,21] Therefore, searching for robust THE that persists in higher temperatures is crucial for potential spintronic applications.

In recent years, the chromium telluride compounds have attracted great interest due to their rich magnetic structures. Some binary Cr_xTe_y family with non-trivial magnetic structures has also been successively discovered since 2022.[16] These Cr_xTe_y compounds are all formed by inserting different concentrations of Cr atoms between the $CrTe_2$ layers along the *a*-axis or *c*-axis.[22] The concentration ratio of Cr atoms plays an important role in the formation of crystal structures, leading to abundant magnetic properties in this family.[23–26] Usually, Cr_2Te_3, Cr_3Te_4, Cr_4Te_5, and Cr_5Te_8 have monoclinic or triangular crystal structures,[23–26] while $Cr_{1.2}Te_2$, CrTe, and $Cr_{1-x}Te$ ($x < 0.1$) crystallize in the form of hexagonal NiAs type.[27–30] The magnetic transition temperature of these binary compounds increases with the increase of Cr content and ultimately exceeds room temperature.[23–31] In previous studies, the highest transition temperature was observed in CrTe and Cr_7Te_8, which reaches 367 K and 361 K, respectively.[32,33] The high Curie temperature and abundant magnetic structure make Cr_xTe_y a potential system searching for chiral or topological magnetic structures which have application potential.

In this study, we synthesized single crystals of $Cr_{0.82}Te$

*Corresponding authors. Email: wlzhen@mail.ustc.edu.cn; qniu@hmfl.ac.cn; tianml@hmfl.ac.cn
© 2024 Chinese Physical Society and IOP Publishing Ltd

with excessive Cr atoms intercalated between monoclinic Cr_4Te_5. The ferromagnetism is further enhanced from 318 K to 340 K while the crystal structure remains the same. The magnetization results reveal clear magnetocrystalline anisotropy with an easy magnetization axis oriented in the *ab* plane. The anomalous Hall effect (AHE) can be well explained by a dominating skew scattering mechanism. Intriguing, after removing the normal Hall effect and anomalous Hall effect, a topological Hall effect can be observed up to 300 K which has not been reported in Cr_4Te_5 single crystals. The THE magnitude can reach up to 1.14 μΩ·cm at 10 K, which is superior to most topological magnetic structural materials. This giant topological Hall effect likely originated from the noncoplanar spin configuration during the spin flop process. Our work has provided a new Cr_xTe_y system to explore novel topological magnetic structures and the great potential for future spintronics.

Experimental Method. Single crystals of $Cr_{0.82}Te$ were grown by a modified chemical vapor transport method. To avoid oxidation of chemical raw materials, the weighing of reagents is carried out in a glove box with oxygen and water content below 0.1 ppm. First, high-purity Cr (99.999%, Alfa Aesar) and Te (99.999%, Alfa Aesar) powder were mixed in a stoichiometric ratio of 1 : 1.1, then sealed in an evacuated silica tube. The quartz tube was placed in a furnace, heated to 1173 K, and held for three days, then cooled slowly to room temperature. Subsequently, the obtained green powder will be re-grounded for at least 30 min, and sealed in an evacuated quartz tube, with iodine used as the transport agent. A dual temperature zone tube furnace was used to grow single crystals in a temperature gradient from 1273 K (source) to 1123 K (sink). The heating process was maintained for ten days, and then the furnace was turned off for natural cooling. Finally, bright plate-like single crystals can be obtained on the sink zone. The single crystal x-ray diffraction (XRD) was carried out using a Rigaku-TTR3 x-ray diffractometer with Cu K_α radiation. Elemental analyses were carried out using a scanning electron microscope (SEM, FEI Helios Nanolab 600i) equipped with an energy-dispersive x-ray spectroscopy (EDS) analyzer (Oxford Inca). The longitudinal and Hall resistivity measurements were performed on a homemade measurement system in Oxford-12 T with a standard six-lead method using silver paste (DuPont, 4929N). The magnetization measurements were carried out on a Quantum Design magnetic properties measurement system (MPMS-7T).

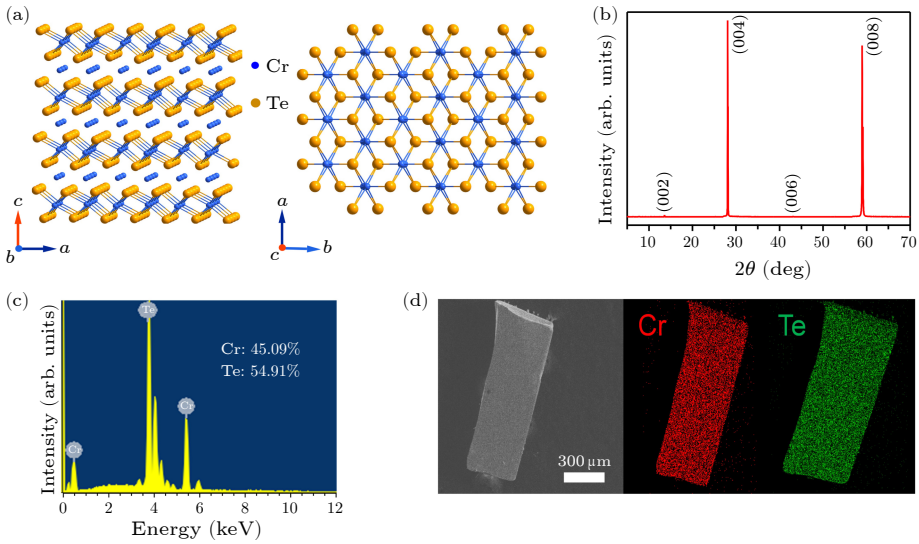

Fig. 1. (a) Different views of crystal structure of $Cr_{0.82}Te$. (b) XRD characterization of the $Cr_{0.82}Te$ single crystal. (c) The stoichiometric ratio of $Cr_{0.82}Te$. (d) SEM image of $Cr_{0.82}Te$ single crystal and EDS elemental mapping.

Figure 1(a) shows the ball stick model of $Cr_{0.82}Te$ crystal under different views. The crystal structure of $Cr_{0.82}Te$ was carefully characterized using single-crystal XRD. Intensity peaks of (00*l*) were observed as shown in Fig. 1(b), indicating the natural growth direction is towards the *c* axis. All diffraction peaks in the XRD pattern can be indexed to the monoclinic structure of the $I2/m$ space group (No. 12) and no additional peaks are observed, suggesting the high quality of the crystal with a pseudo-NiAs type structure. The interplanar spacing of the *c*-axis direction is calculated to be 12.716 ± 0.03 Å. The lattice constant *c* is very close to Cr_3Te_4 (c = 12.297 Å) with the same crystal structure ($I2/m$).[24] Therefore, $Cr_{0.82}Te$ can be considered as a monoclinic system of Cr_3Te_4, with more Cr atoms intercalation, which is also consistent with the shift from the XRD diffraction peak to a lower angle. The EDS measurement acquired on the surface of an as-grown $Cr_{0.82}Te$ single crystal is shown in Fig. 1(c). The chemical composition is Cr : Te = 45.09% : 54.91%, close to a stoichiometric ratio of 0.82 : 1. The surface of the grown single crystal is very smooth, and Cr and Te elements are spatially uniformly distributed, as shown by the SEM image and EDS elemental mapping in Fig. 1(d). EDS measurements on more crystals are also presented in Fig. S1 in the Supplementary Materials, which all have a stoichiometric ratio close to 0.82 : 1.

To characterize the magnetic properties of $Cr_{0.82}Te$ single crystal, magnetization measurements (M–T) have been investigated in the range of 2–400 K. Figures 2(a) and 2(b) show the magnetization of $Cr_{0.82}Te$ single crystal as a function of temperature at different magnetic field magnitudes (50 Oe, 1000 Oe, and 2000 Oe), with H along the ab plane and c axis, respectively. As temperature decreases, a paramagnetic-to-ferromagnetic transition is detected in both field directions. From the first derivative of magnetization (dM/dT), as shown in Fig. S2, the transition temperature can be located at approximately 340 K (T_c). The T_c exceeds those of the vast majority of Cr_xTe_y compounds with similar crystal structures (Cr_5Te_8, Cr_3Te_4, and $Cr_{4.14}Te_8$), which may be attributed to more Cr atoms intercalation.[24,26,34] The interaction between interlayer Cr atoms and intralayer Cr atoms occurs through the $5p$ orbitals of Te atoms.[35] This indirect exchange interaction increases the Curie temperature and enhances the in-plane ferromagnetic coupling as well. In addition, as shown in Fig. 2(c), the zero-field-cooling (ZFC) and field-cooling (FC) curves will depart from each other as the temperature decreases when a relatively small magnetic field is applied in both directions, which has also been reported in Cr_4Te_5 and Cr_5Te_8 and attributed to the appearance of canted antiferromagnetic (AFM) structure.[25,26] This AFM magnetic structure is sensitive to the Cr atom concentration, as a higher Cr ratio will lead to a transition temperature closer to T_c.[25] When the magnetic field increases, this AFM phase will also be suppressed rapidly as shown in Figs. 2(a) and 2(b). Intriguingly, as the temperature further cooling, the out-of-plane magnetization decreases sharply near 100 K (T_s), while the in-plane magnetization increases slightly, indicating a new magnetic structure transition. This feature has rarely been observed in other Cr-Te series compounds with the same crystal structure, suggesting the crucial role of the excess Cr intercalation in the evolution of magnetic structures. We provide a more detailed explanation of the magnetic structure transition near T_s (Supplementary Materials, Section 3).

The isothermal field-dependent magnetization (M–H) curves at various temperatures measured in $H||ab$-plane and $H||c$-axis are used to further explore the magnetic ground state. As shown in Figs. 2(d) and 2(e), the $Cr_{0.82}Te$ single crystal shows a soft ferromagnet characteristic as its coercive field can be ignored and no obvious hysteresis loop is detected. The magnitudes of the in-plane and out-of-plane saturated magnetic fields shown in Fig. 2(f) at $T = 300$ K are 0.4 T and 1.5 T, respectively, indicating an in-plane easy magnetization axis. Significant differences in saturated magnetic fields were observed in different magnetic field directions, which strongly proves the existence of magnetic anisotropy. The extracted saturation magnetic moments (M_s) of $Cr_{0.82}Te$ single crystal at 2 K for $H||ab$-plane and $H||c$-axis are 2.867 μ_B/Cr and 2.841 μ_B/Cr, respectively, which are larger than the M_s values in Cr_5Te_8 (1.57 μ_B/Cr) and Cr_4Te_5 (2.64 μ_B/Cr), but less than the standard M_s of Cr-free ion (3 μ_B/Cr) according to the ionic model, indicating an itinerant nature of the d-electrons and the presence of electron-correlation effect.[25] The increase in Cr content is also responsible for the stronger itinerancy, which leads to the relatively large M_s for $Cr_{0.82}Te$ single crystal in this work.

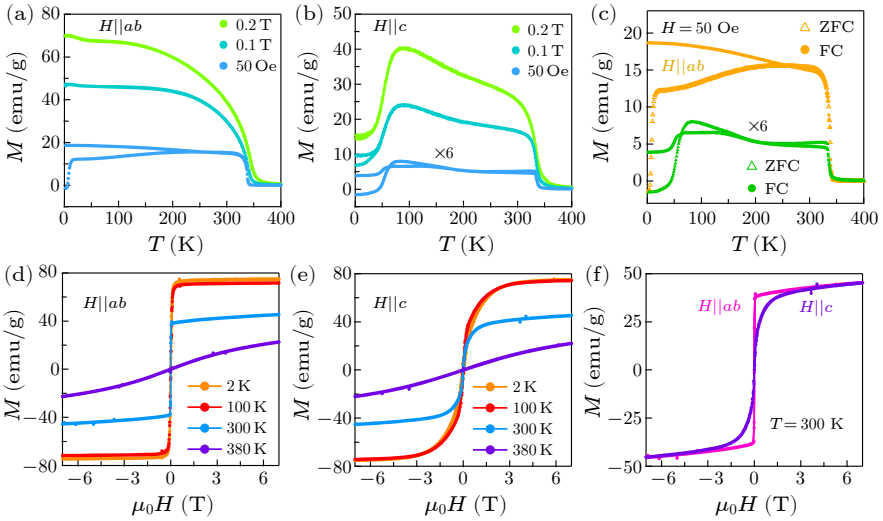

Fig. 2. [(a), (b)] Temperature dependence of magnetization with various magnetic field, under $H||ab$ and $H||c$, respectively. (c) Temperature dependence of magnetization with a magnetic field $H = 50$ Oe for $H||ab$ and $H||c$. [(d), (e)] Magnetic field dependence of magnetization with different temperatures for $H||ab$ and $H||c$, respectively. (f) Magnetic field dependence of magnetization at 300 K for $H||ab$ and $H||c$.

For itinerant magnetic systems, the coupling of charge and spin of electrons usually gives rise to exotic magnetotransport behaviors.[36] To further understand the evolution of magnetic structures, we carried out a systematic study of the magnetotransport properties. Figure 3(a) presents a schematic diagram of the magnetotransport measurement of $Cr_{0.82}Te$ single crystal in a standard six-lead method. The size of the single crystal used for the experiment is $1000 \times 600 \times 60\ \mu m^3$ (length × width × height) and the current is applied in ab plane. As shown in

Fig. 3(b), the temperature-dependent longitudinal resistance (R_{xx}) exhibits typical metallic behavior upon cooling from 400 K to 2 K. The dR/dT curve shows a significant slope change at 344 K, consistent with the paramagnetic-to-ferromagnetic transition temperature T_c observed in the M–T curves. According to the renormalized spin fluctuation theory, the R_{xx} in itinerant ferromagnetism exhibits a T^2 dependence. In $Cr_{0.82}Te$ single crystals, the $R(T)$ curve shows a more accurate fitting outcome by adding an $aT^{3/2}$ term contributed by spin fluctuation scattering, $R(T) = R_0 + aT^{3/2} + bT^2$, where R_0 is the residual resistance, a and b are constants.[37] The fitting gives $R_0 = 0.0497\,\Omega$, $a = 7.1 \times 10^{-6}\,\Omega{\cdot}K^{-3/2}$, and $b = -4.8 \times 10^{-8}\,\Omega{\cdot}K^{-2}$, respectively, indicating a dominating $T^{3/2}$ item. Therefore, it is necessary to consider strong electron correlation in the transport results of $Cr_{0.82}Te$ single crystal.

Figure 3(c) shows the magnetoresistance (MR) of the $Cr_{0.82}Te$ single crystal at different temperatures when the magnetic field is applied along the ab plane and c axis, respectively. Here MR was defined as $\frac{1}{R_{xx}(0)}[R_{xx}(\mu_0 H) - R_{xx}(0)] \times 100\%$. The MR is negative and shows no sign of saturation up to 12 T at all temperatures, which may be related to spin-dependent scattering.[38] When the temperature is lower than T_c, a negative MR peak was observed at low field for both directions. This peak disappears at temperature exceeding 350 K, which is consistent with the paramagnetic-to-ferromagnetic transition. As the magnetic field further increases, the slope of the negative MR curve changes, which can be attributed to the saturation of M_s as shown in Fig. 3(d). The negative MR value is plotted in Fig. 3(e) as a function of temperature. It is clear that the negative MR is temperature dependent and most pronounced near T_c, indicating that the negative MR originates from suppressing spin disorder scattering under an external magnetic field.

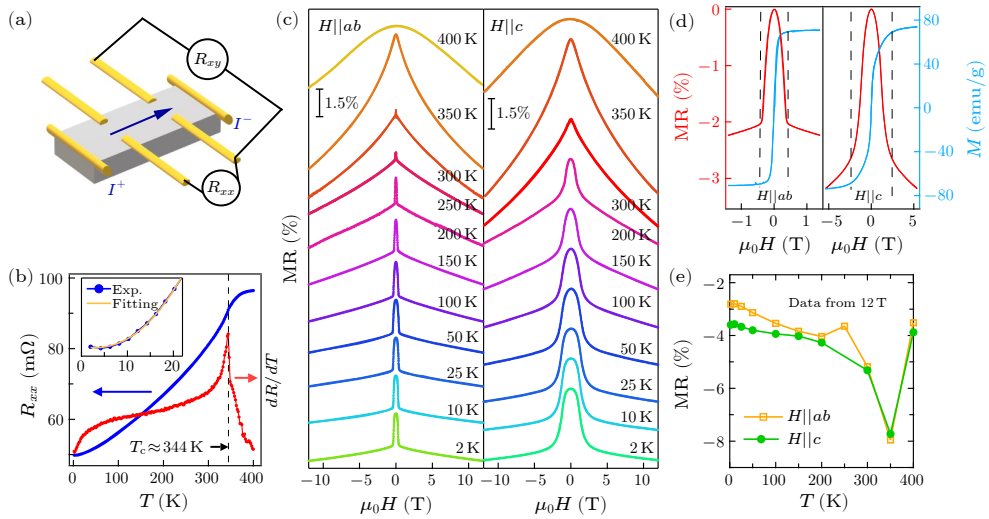

Fig. 3. (a) Schematic of R_{xx} and R_{xy}. (b) Temperature dependence of longitudinal resistance (blue line). The inset shows low-temperature resistance fitting line. The red line presents differential resistance (dR/dT) with temperature for $Cr_{0.82}Te$ crystal. (c) Magnetoresistance measured at various temperatures from 2 K to 400 K for $H||ab$ (left) and $H||c$ (right). (d) Magnetic field dependence of MR (red line) and magnetization (blue line) at 100 K for $H||ab$ and $H||c$, respectively. (e) Temperature dependence of magnetoresistance for $H||ab$ and $H||c$. Data obtained from 12 T in (c).

Figure 4(a) shows the magnetic field dependence of R_{xy} at different temperatures with $I||ab$-plane and $H||c$-axis. Due to the soft ferromagnetism of $Cr_{0.82}Te$, R_{xy} does not exhibit a hysteresis loop at low field. When the sample was fully polarized in a high field limit, R_{xy} gradually saturated, demonstrating the presence of an anomalous Hall effect in $Cr_{0.82}Te$. Intriguingly, near the saturated magnetic field, an anomalous peak is also observed, which has also been reported in several other magnetic materials with nontrivial spin configurations.[8,13–16] Typically, the total Hall resistance R_{xy} can be described by the formula $R_{xy} = R^{N}_{xy} + R^{A}_{xy} = R_n \mu_0 H + R_S M$, where R_n and R_S are the normal and AHE coefficients, respectively.[34] The normal Hall resistance can be estimated by linear fitting to the field-dependent R_{xy} in high magnetic field limit, while the R^{A}_{xy} part, which is linearly proportional to M, can be obtained from the M–H relation. However, after these two terms removed, there is still an additional Hall component as shown in Fig. 4(b). This Hall component, i.e., $R^{U}_{xy} = R_{xy} - R_n \mu_0 H - R_S M$, is usually called topological Hall effect.[16,39]

The extracted R^{U}_{xy} values at different temperatures are displayed in Fig. 4(c) as a function of magnetic field. They exhibit hump-like shapes when the field was applied, and gradually were suppressed in the polarized state. Here we define the maximum value as R^{U-peak}_{xy} and its corresponded magnetic field value as H^{peak}_c. The R^{U-peak}_{xy} is strongly temperature dependent and gradually suppressed as the temperature approaches T_c due to spin fluctuation and thermal fluctuation. Intriguingly, the H^{peak}_c reaches a broad maximum value at 100 K, where we detected the T_s from the M–T curve shown in Fig. 2(a). Meanwhile,

we also extracted the carrier information from the R_{xy}^{N}, which gives hole-type carriers with the carrier concentration n around $6.99 \times 10^{21}\mathrm{cm}^{-3}$ at 2 K. When temperature increases, n also shows a maximum at T_{s} as shown in Fig. 4(e). These evidences indicate that the localized spin and itinerant electrons are coupled to each other in this material and the magnetic transition near T_{S} significantly influences the density of electronic states near the Fermi surface.

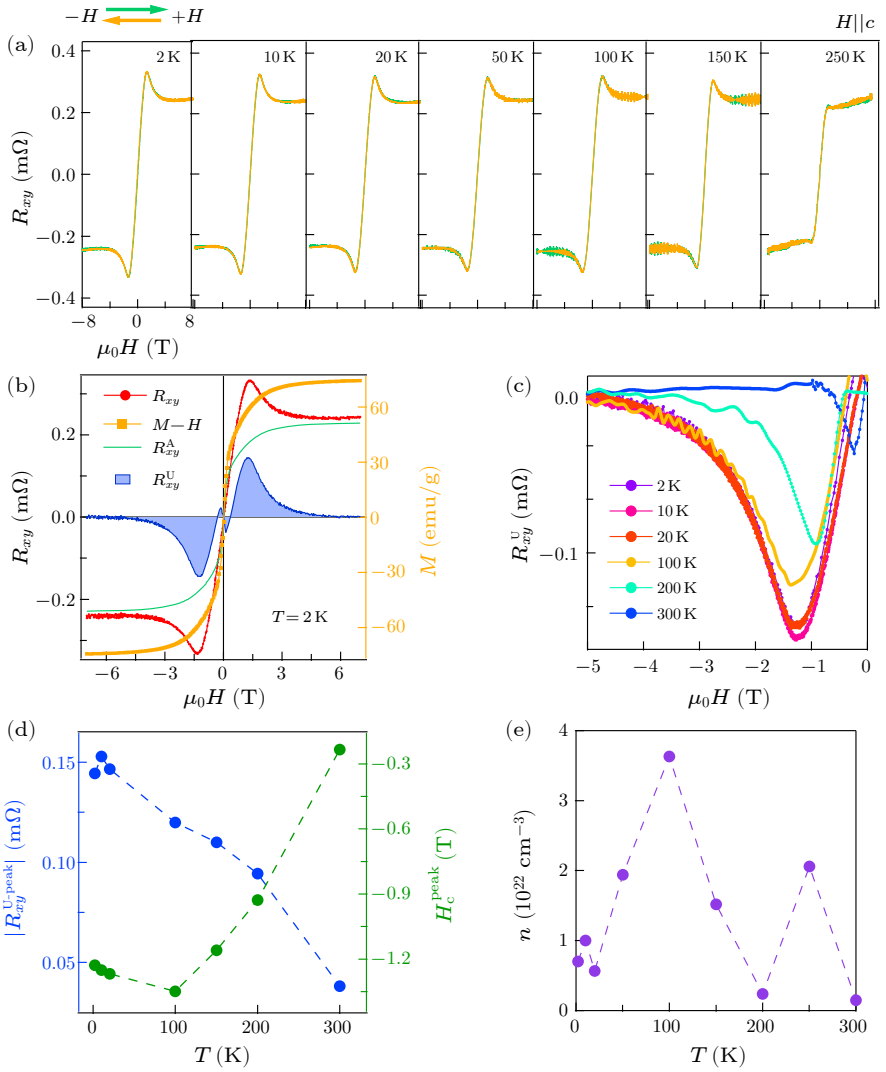

Fig. 4. (a) R_{xy} curve at various temperatures. (b) Magnetic field dependence of R_{xy}, M, R_{xy}^{A}, and R_{xy}^{U} at 2 K. (c) Magnetic field dependence of R_{xy}^{U} at various temperatures. (d) $R_{xy}^{\mathrm{U-peak}}$ (blue line) and $H_{\mathrm{c}}^{\mathrm{peak}}$ (green line) as a function of temperature. (e) Variation of carrier concentration with temperature.

The AHE can be attributed to two distinct mechanisms: intrinsic effect influenced by the non-zero Berry curvature in the momentum space and extrinsic effect caused by either skew or side-jump scattering.[40] The proportional relationship between anomalous Hall conductivity (σ_{xy}^{A}) and longitudinal conductivity (σ_{xx}) can be used to identify the AHE mechanism. The σ_{xy}^{A} caused by Berry curvature is usually limited by e^2/ha (e is the electronic charge, h is the Planck constant, and a is the lattice constant) with a magnitude of 10^2–$10^3\,\Omega^{-1}\cdot\mathrm{cm}^{-1}$.[41] In this case, σ_{xy}^{A} is independent of the σ_{xx}, and typically remains a constant.[42] However, if σ_{xy}^{A} results from skew scattering, σ_{xy}^{A} will be linearly dependent on σ_{xx}.[43]

In Fig. 5(a), we fit σ_{xy}^{A} and σ_{xx} in $Cr_{0.82}Te$ with a power law function and get a linear dependence with m close to 1, suggesting that the AHE mechanism is dominated by extrinsic skew scattering. At the same time, σ_{xy}^{A} also shows a strong temperature dependence. As the temperature rises, σ_{xy}^{A} decreases and gradually disappears near T_{c}. Typically, for metals in the clean limit, σ_{xy}^{A} is of the order of 10^3–$10^5\,\Omega^{-1}\cdot\mathrm{cm}^{-1}$.[43] However, we note that the calculated value of σ_{xy}^{A} in this system approximates $30\,\Omega^{-1}\cdot\mathrm{cm}^{-1}$. Such a small σ_{xy}^{A} in $Cr_{0.82}Te$ implies that impurity scattering occupies a large contribution to the overall AHE and $Cr_{0.82}Te$ is located in the skew scattering dirty limit.[34,44]

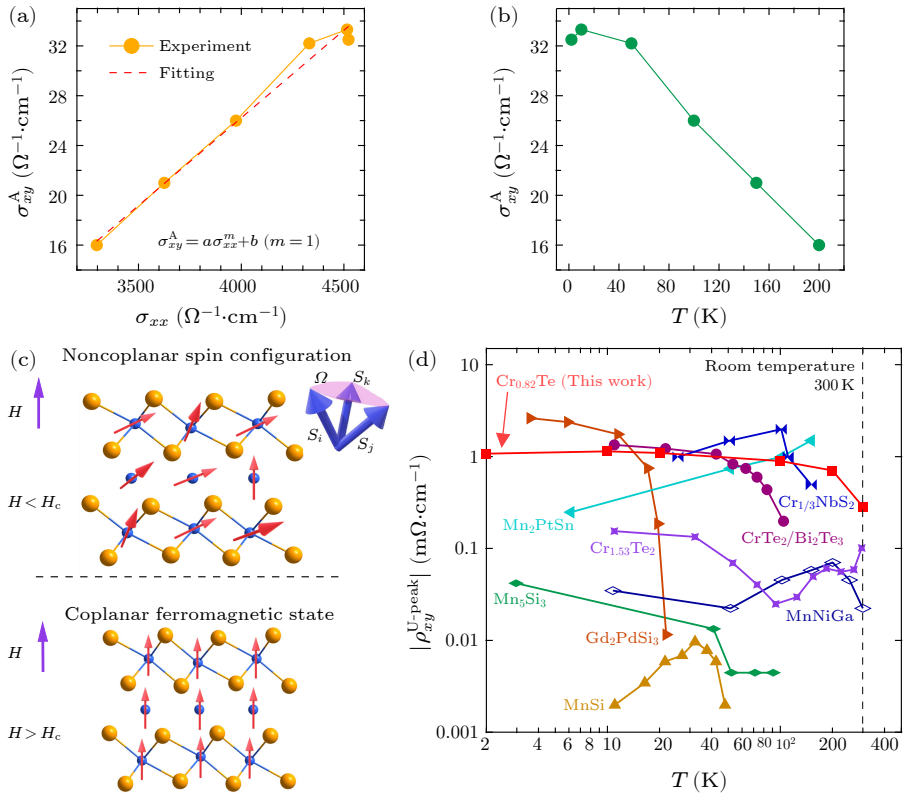

Fig. 5. (a) σ_{xx} dependence of σ_{xy}^{A}. The dashed line in (a) represents a fit line with the equation shown on the figure. (b) Temperature dependence of σ_{xy}^{A}. (c) The spin configurations of $Cr_{0.82}Te$ single crystal with different out-of-plane magnetic fields. Inset: schematic diagram of scalar spin chirality. (d) Comparison of the ρ_{xy}^{U-peak} among various materials. The black dotted line represents the room temperature.

Finally, we discuss the connection between the THE and the spin configuration. The hump-like shaped Hall effect cannot be described simply by a collinear ferromagnetic structure. Recently, in self-intercalated $Cr_{1+x}Te_2$ compounds with the same crystal structure as $Cr_{0.82}Te$, noncoplanar magnetic structures and magnetic skyrmions were discovered through Lorentz transmission electron microscopy (L-TEM), and topological Hall effects were also observed in magnetoelectric transport.[45] These experiments indicate that there may also be noncoplanar magnetic structures or topological non-trivial magnetic structures in $Cr_{0.82}Te$. We note that the THE only appears in the region where H is less than the saturated magnetic field of c-axis (H_c) but persists for a large temperature range from 2 K to room temperature. When an external magnetic field is applied, the spin on the Cr sublattice will flop from the ab plane to the c axis, suggesting that THE can exist in the magnetic state with noncoplanar spin structure. The noncoplanar spin configuration will induce Dzyaloshinskii–Moriya interaction (DMI), thereby contributing to THE.[13] We have discussed the contribution of DM interaction to the generation of THE in $Cr_{0.82}Te$ crystal (see Section 4 in the Supplementary Materials). Generally, DMI occurs in non-centrosymmetric magnetic materials.[7] However, DMI can still be present in materials that belong to centrosymmetric space groups but possess strong magnetic anisotropy.[46] $Cr_{0.82}Te$ has a monoclinic structure and strong uniaxial magnetic anisotropy (see Section 5 in the Supplementary Materials), enabling the existence of DMI in its single crystals. Figure 5(c) shows the phenomenological schematic diagram of Cr spin configuration at different magnetic field magnitudes when H is along the c axis. When $H < H_c$, the magnetic structure of $Cr_{0.82}Te$ may be a noncoplanar spin configuration with scalar spin chirality ($S_i \cdot (S_j \times S_k) \neq 0$), which will endow itinerant electrons with a phase factor and act as a fictitious magnetic field $\boldsymbol{b}$. The $\boldsymbol{b}$ deflects the motion of charge carriers, leading to the THE response. As the magnetic field further increases ($H > H_c$), the spin structure arrangement is consistent and enters a saturated ferromagnetic state. The precise magnetic structure can be further confirmed by neutron scattering or L-TEM in the future. Figure 5(d) summarizes the magnitudes of THE observed at different temperatures in $Cr_{0.82}Te$ and some representative materials.[45,47–53] Our $Cr_{0.82}Te$ single crystal exhibits a remarkably high THE with a maximum value of approximately 1.14 μΩ·cm. These high values exceed the majority of materials with topological magnetic structures. Additionally, the large THE can be maintained across a wider temperature range of 2–300 K, which suggests potential for future use in spintronic applications.

In summary, we have grown monoclinic $Cr_{0.82}Te$ single crystals using chemical vapor transport method, and systematically studied their crystal structure, magnetic properties, electric transports and Hall effect. The Curie temperature is increased to around 340 K with excess Cr

atom intercalation and a new magnetic transition is discovered at T_S around 100 K. The *ab* plane is oriented in the easy-axis plane, inducing a significant magnetocrystalline anisotropy. Below T_s, the in-plane magnetization increases slightly while the out-of-plane magnetization decreases sharply. Additionally, a large AHE and THE exist and persist up to 300 K. The linear scaling law of σ_{xy}^{A} and σ_{xx} and small σ_{xy}^{A} reveal that the AHE mechanism is dominated by extrinsic skew scattering with the dirty limit. The THE can be attributed to the DMI induced by noncoplanar spin configuration during the spin flop process when H is applied to the c axis. These results imply that the THE can be present in centrosymmetric space group with strong magnetocrystalline anisotropy. Neutron scattering or L-TEM experiments are desired to confirm the precise magnetic structure in the future. This work has revealed the remarkable THE in $Cr_{0.82}Te$ that persists up to room temperature, demonstrating significant potential for future spintronic devices applications.

Acknowledgements. This work was supported by the National Key R&D Program of China (Grant No. 2022YFA1602603), the Basic Research Program of the Chinese Academy of Sciences Based on Major Scientific Infrastructures (Grant No. JZHKYPT-2021-08), the National Natural Science Foundation of China (Grant No. 12104459), and the Excellent Program of Hefei Science Center CAS (Grant No. 2021HSC-CIP016).

References

[1] Gutfleisch O, Willard M A, Brück E, Chen C H, Sankar S G, and Liu J P 2011 *Adv. Mater.* **23** 821
[2] Slaughter J M 2009 *Annu. Rev. Mater. Sci.* **39** 277
[3] Luo W, Zhu L L, and Zheng X J 2009 *Chin. Phys. Lett.* **26** 117502
[4] Stiles M D and Zangwill A 2002 *Phys. Rev. B* **66** 014407
[5] Manchon A, Železný J, Miron I M, Jungwirth T, Sinova J, Thiaville A, Garello K, and Gambardella P 2019 *Rev. Mod. Phys.* **91** 035004
[6] Karube K, White J S, Reynolds N, Gavilano J L, Oike H, Kikkawa A, Kagawa F, Tokunaga Y, Rønnow H M, Tokura Y, and Taguchi Y 2016 *Nat. Mater.* **15** 1237
[7] Yu X Z, Onose Y, Kanazawa N, Park J H, Han J H, Matsui Y, Nagaosa N, and Tokura Y 2010 *Nature* **465** 901
[8] Wang W, Zhao Y F, Wang F, Daniels M W, Chang C Z, Zang J, Xiao D, and Wu W 2021 *Nano Lett.* **21** 1108
[9] Tokunaga Y, Yu X Z, White J S, Rønnow H M, Morikawa D, Taguchi Y, and Tokura Y 2015 *Nat. Commun.* **6** 7638
[10] Togawa Y, Koyama T, Takayanagi K, Mori S, Kousaka Y, Akimitsu J, Nishihara S, Inoue K, Ovchinnikov A S, and Kishine J 2012 *Phys. Rev. Lett.* **108** 107202
[11] Zhou Y, Iacocca E, Awad A A, Dumas R K, Zhang F C, Braun H B, and Åkerman J 2015 *Nat. Commun.* **6** 8193
[12] Vistoli L, Wang W, Sander A, Zhu Q, Casals B, Cichelero R, Barthélémy A, Fusil S, Herranz G, Valencia S, Abrudan R, Weschke E, Nakazawa K, Kohno H, Santamaria J, Wu W, Garcia V, and Bibes M 2019 *Nat. Phys.* **15** 67
[13] Zhang G, Luo Q, Wen X, Wu H, Yang L, Jin W, Li L, Zhang J, Zhang W, Shu H, and Chang H 2023 *Chin. Phys. Lett.* **40** 117501
[14] Raju M, Petrović A P, Yagil A, Denisov K S, Duong N K, Göbel B, Şaşıoğlu E, Auslaender O M, Mertig I, Rozhansky I V, and Panagopoulos C 2021 *Nat. Commun.* **12** 2758
[15] Liang D, DeGrave J P, Stolt M J, Tokura Y, and Jin S 2015 *Nat. Commun.* **6** 8217
[16] Zhang C, Liu C, Zhang J, Yuan Y, Wen Y, Li Y, Zheng D, Zhang Q, Hou Z, Yin G, Liu K, Peng Y, and Zhang X X 2023 *Adv. Mater.* **35** 2205967
[17] Li S, Kang W, Zhang X, Nie T, Zhou Y, Wang K L, and Zhao W 2021 *Mater. Horizons* **8** 854
[18] Zhang X C, Zhou Y, Mee Song K, Park T E, Xia J, Ezawa M, Liu X X, Zhao W S, Zhao G P, and Woo S 2020 *J. Phys.: Condens. Matter* **32** 143001
[19] Yang S, Moon K W, Ju T S, Kim C, Kim H J, Kim J, Tran B X, Hong J I, and Hwang C 2021 *Adv. Mater.* **33** 2104406
[20] Huang M, Gao L, Zhang Y, Lei X, Hu G, Xiang J, Zeng H, Fu X, Zhang Z, Chai G, Peng Y, Lu Y, Du H, Chen G, Zang J, and Xiang B 2021 *Nano Lett.* **21** 4280
[21] Zheng X, Zhao X, Qi J, Luo X, Ma S, Chen C, Zeng H, Yu G, Fang N, Rehman S U, Ren W, Li B, and Zhong Z 2021 *Appl. Phys. Lett.* **118** 072402
[22] Dijkstra J, Weitering H H, van Bruggen C F, Haas C, and de Groot R A 1989 *J. Phys.: Condens. Matter* **1** 9141
[23] Wen Y, Liu Z H, Zhang Y, Xia C X, Zhai B X, Zhang X H, Zhai G H, Shen C, He P, Cheng R Q, Yin L, Yao Y Y, Getaye Sendeku M, Wang Z X, Ye X B, Liu C S, Jiang C, Shan C X, Long Y W, and He J 2020 *Nano Lett.* **20** 3130
[24] Wang A, Rahman A, Du Z, Zhao J, Meng F, Liu W, Fan J, Ma C, Ge M, Pi L, Zhang L, and Zhang Y 2023 *Phys. Rev. B* **108** 094429
[25] Zhang L Z, Zhang A L, He X D, Ben X W, Xiao Q L, Lu W L, Chen F, Feng Z, Cao S, Zhang J, and Ge J Y 2020 *Phys. Rev. B* **101** 214413
[26] Zhu W, Ma Z, Yan J, Zheng G, Cheng L, Xu X, Meng Z, Shen L, An K, Zhou C, Qu Z, Luo X, Sun Y, Zhang Z, and Sheng Z 2020 *J. Magn. Magn. Mater.* **512** 167019
[27] Ma X, Huang M, Wang S, Liu P, Zhang Y, Lu Y, and Xiang B 2023 *ACS Appl. Electron. Mater.* **5** 2838
[28] Li C, Liu K, Jiang D, Jin C, Pei T, Wen T, Yue B, and Wang Y 2022 *Inorg. Chem.* **61** 14641
[29] Takagaki M, Kawakami T, Tanaka N, Shirai M, and Motizuki K 1998 *J. Phys. Soc. Jpn.* **67** 1014
[30] Sun S, Liang J, Liu R, Shen W, Wu H, Tian M, Cao L, Yang Y, Huang Z, Lin W, Du J, Ni Z, Xu Y, Chen Q, and Zhai Y 2022 *J. Alloys Compd.* **890** 161818
[31] Shu Z, Wang H, Jo N H, Jozwiak C, Bostwick A, Rotenberg E, Xie W, and Kong T 2023 *Phys. Rev. Mater.* **7** 044406
[32] Liu J, Ding B, Liang J J, Li X, Yao Y, and Wang W H 2022 *ACS Nano* **16** 13911
[33] Hashimoto T and Yamaguchi M 1969 *J. Phys. Soc. Jpn.* **27** 1121
[34] Yan J, Luo X, Lin G, Chen F, Gao J, Sun Y, Hu L, Tong P, Song W, Sheng Z, Lu W, Zhu X, and Sun Y 2018 *Europhys. Lett.* **124** 67005
[35] Zhang X, Liu W, Niu W, Lu Q, Wang W, Sarikhani A, Wu X, Zhu C, Sun J, Vaninger M, Miceli P F, Li J, Singh D J, Hor Y S, Zhao Y, Liu C, He L, Zhang R, Bian G, Yu D, and Xu Y 2022 *Adv. Funct. Mater.* **32** 2202977
[36] Deng Y, Xiang Z, Lei B, Zhu K, Mu H, Zhuo W, Hua X, Wang M, Wang Z, Wang G, Tian M, and Chen X 2022 *Nano Lett.* **22** 9839
[37] Liu Y, Tan H, Hu Z, Yan B, and Petrovic C 2021 *Phys. Rev. B* **103** 045106
[38] Yamada H and Takada S 1972 *Prog. Theor. Exp. Phys.* **48** 1828
[39] Miao W, Zhen W, Tan C, Wang J, Nie Y, Wang H, Wang L, Niu Q, and Tian M 2023 *ACS Nano* **17** 25449
[40] Nagaosa N, Sinova J, Onoda S, MacDonald A H, and Ong N P 2010 *Rev. Mod. Phys.* **82** 1539
[41] Onoda S, Sugimoto N, and Nagaosa N 2008 *Phys. Rev. B* **77** 165103
[42] Miyasato T, Abe N, Fujii T, Asamitsu A, Onoda S, Onose Y, Nagaosa N, and Tokura Y 2007 *Phys. Rev. Lett.* **99** 086602
[43] Huang M, Wang S, Wang Z, Liu P, Xiang J, Feng C, Wang X, Zhang Z, Wen Z, Xu H, Yu G, Lu Y, Zhao W, Yang S A, Hou D, and Xiang B 2021 *ACS Nano* **15** 9759

[44] Purwar S, Low A, Bose A, Narayan A and Thirupathaiah S 2023 *Phys. Rev. Mater.* **7** 094204

[45] Saha R, Meyerheim H L, Göbel B, Hazra B K, Deniz H, Mohseni K, Antonov V, Ernst A, Knyazev D, Bedoya-Pinto A, Mertig I, and Parkin S S P 2022 *Nat. Commun.* **13** 3965

[46] Nakamura M, Morikawa D, Yu X Z, Kagawa F, Arima T H, Tokura Y, and Kawasaki M 2018 *J. Phys. Soc. Jpn.* **87** 074704

[47] Kurumaji T, Nakajima T, Hirschberger M, Kikkawa A, Yamasaki Y, Sagayama H, Nakao H, Taguchi Y, Arima T H, and Tokura Y 2019 *Science* **365** 914

[48] Liu Z H, Burigu A, Zhang Y J, Jafri H M, Ma X Q, Liu E K, Wang W H, and Wu G H 2018 *Scr. Mater.* **143** 122

[49] Sürgers C, Fischer G, Winkel P, and Löhneysen H v 2014 *Nat. Commun.* **5** 3400

[50] Li Y, Kanazawa N, Yu X Z, Tsukazaki A, Kawasaki M, Ichikawa M, Jin X F, Kagawa F, and Tokura Y 2013 *Phys. Rev. Lett.* **110** 117202

[51] Zhang X Q, Ambhire S C, Lu Q S, Niu W, Cook J, Jiang J S, Hong D S, Alahmed L, He L, Zhang R, Xu Y B, Zhang S S L, Li P, and Bian G 2021 *ACS Nano* **15** 15710

[52] Hall A E, Loudon J C, Midgley P A, Twitchett-Harrison A C, Holt S J R, Mayoh D A, Tidey J P, Han Y, Lees M R, and Balakrishnan G 2022 *Phys. Rev. Mater.* **6** 024407

[53] Wang W, Zhang Y, Xu G, Peng L, Ding B, Wang Y, Hou Z, Zhang X, Li X, Liu E, Wang S, Cai J, Wang F, Li J, Hu F, Wu G, Shen B, and Zhang X X 2016 *Adv. Mater.* **28** 6887